EXPERIMENTAL VALIDATION OF TILT-ROTOR AERODYNAMIC PREDICTIONS

J. Decours[1], P. Beaumier[1], W. Khier[2], T. Kneisch[3], M. Valentini[4], L. Vigevano[4]

[1] ONERA, Meudon, France [2] DLR, Braunschweig, Germany [3] Airbus Helicopters Deutschland, Donauwörth, Germany [4] Dipartimento di Scienze e Tecnologie Aerospaziali - Politecnico di Milano, Italy

Abstract

A comparison of experimental data with several numerical predictions of the aerodynamic loads on the ERICA model is presented. The calculations are carried out by several Partners of the NICETRIP consortium, with different codes, turbulence models and grids, with the objective of validating the predictive capability of the CFD tools. Concerning the highly loaded minimum speed aircraft mode AC1, a large separation on the wings has been shown, both by experimental measurements and CFD simulations. Despite this large separation, a good agreement has been obtained between CFD simulations and wind tunnel measurements. Strong aerodynamic interactions between the 4/rev. blades passage and the tiltable wing, the nacelle and the fixed wing loads have been confirmed. Finally, we recommend increasing the aircraft speed flight and reducing the angle of attack for this configuration in order to avoid flow separation and reduce aircraft vibrations. In the highly loaded conversion mode CC4, a good agreement between CFD and experimental results has also been shown, in addition to 4/rev. loads fluctuations leading to aircraft vibrations.

1 Introduction

In the framework of the NICETRIP European project, a highly sophisticated and motorized, 1:5 scale model of the ERICA (Enhanced Rotorcraft Innovative Concept Achievement) tilt-rotor design has been manufactured and assembled for experimental test campaigns carried out in the 9.5 x 9.5m test section of the DNW-LLF wind tunnel and in the 8m diameter ONERA S1MA wind tunnel. The conversion corridor configurations have been tested in the DNW-LLF wind tunnel, from helicopter mode (nacelles tilted at 90 degrees) to very low speed aircraft mode at M=0.17 (nacelles not tilted). A conversion configuration is presented in the DNW-LLF wind tunnel in figure 1. In the ONERA S1MA wind tunnel, configurations from the end of conversion (CC4, nacelles tilted at 30 degrees) at M=0.17 to very high speed aircraft mode at M=0.55 (nacelles not tilted) have been tested. An aircraft configuration is presented in the ONERA S1MA wind tunnel in figure 2.

Preliminary, pre-test numerical simulations of the low speed aircraft-mode configuration (AC1) at zero incidence [1], carried out by the Partners of the NICETRIP consortium with different CFD codes, showed that the overall qualitative agreement of the pressure distributions among different calculations was somewhat acceptable, while the scatter of the quantitative average loads was still important.

Figure 1: Conversion configuration in the DNW-LLF wind tunnel.

Figure 2: Aircraft configuration in the ONERA S1MA wind tunnel.

The present work aims at further evaluating the prediction capability of the Partners' CFD tools through the comparison of the numerical simulations with the experimental global loads and pressure distributions gathered in both DNW-LLF and ONERA S1MA wind tunnels. Two different configurations are considered, among those measured in the wind tunnel. The first configuration refers to the very low speed aircraft-mode operation at M=0.17 at a large angle of attack of 9.9 degrees ($Re=1.7*10^6$, based on the model wing mean chord); this case is labeled AC1. The second configuration represents a typical example of conversion corridor operation mode, at the same Mach number, featuring a small (4 degrees) rotation of the outer wing, a significant (30 degrees) rotation of the nacelles and an aircraft angle of attack of 5.2 degrees; it is labeled CC4.

As for the pre-test simulations, time-accurate unsteady calculations were performed by ONERA with the ***elsA*** code, DLR with the FLOWer code, Politecnico di Milano (PoliMi) with the ROSITA code, while unsteady calculations with an uniformly loaded Actuator Disk (AD) rotor model were completed by Airbus Helicopters Deutschland (AHD) with the FLOWer code. All Partners simulated the ERICA model in the DNW-LLF tunnel with a belly support sting, though with different grid settings. All Chimera grid systems have been generated so as to allow the calculation of different geometrical configurations, as required for the conversion operating conditions of the tiltrotor aircraft.

The paper presents a detailed analysis and comparison of the achieved results, which allow assessing the relative influence of the numerical methods, turbulence models and grids on the aerodynamic loads and flow field features. It is organized as follows: section 2 briefly recalls the characteristic of the employed CFD solvers and describes the numerical parameters of the simulations and the grid systems used; the achieved numerical results are then compared and discussed in section 3 and the conclusions of the comparison exercise are drawn in the last section.

2 Numerical details

The numerical simulations presented and discussed hereinafter are based on the time-accurate solution of the Unsteady Reynolds (Favre) Averaged Navier-Stokes (URANS) equations in three dimensions by means of three CFD codes: ***elsA*** [2] by ONERA, FLOWer [3] by DLR and AHD, and ROSITA [4] by PoliMi. These codes represent the state-of-the-art in Europe for helicopter aerodynamic simulations using the block-structured grid, finite volume, Chimera approach. The similarity and differences of the numerical methods employed have been outlined in [1] and will not be repeated here. For the following discussion, it is only worth recalling the turbulence models [5, 6, 7, 8] used by the different Partners in the simulations, as done in Table 1.

All grids were generated to represent the ERICA model mounted on the ventral sting configuration tested in the 9.5*9.5m test section of the DNW-LLF wind tunnel, see Figure 3.

The overlapping grid assembly generated by ONERA is characterized by the small extension (about 1 chord), away from the solid surface, of the fuselage and wing grids, and the large extension of the nacelle grid, which encompasses almost entirely the rotor diameter and the tiltable wing, for wake and interactions capturing purposes. A Cartesian background grid completes the system up to the wind tunnel walls. The grid system allows for a 2 mm gap between fixed and tiltable wing so as to the nacelle and tiltable wing gap and fully represents the blade root, leaving a small gap between blade and spinner.

PoliMi took advantage of the ONERA grid system for the AC1 case. However, for the CC4 case some modifications were required to cope with a different tagging algorithm. The nacelle grid was made finer and two auxiliary grids, located in the regions of the fixed/tiltable wings and tiltable wing/nacelle junctions, were introduced.

Independently generated overlapping grid sets were used by DLR and AHD. The grid set generated by DLR accounts for a 1 mm gap between fixed and tiltable wing and does not represents the blade root. AHD calculations have been carried out with a slightly modified version of DLR grid, which accounts for a local refinement in the interwing gap region in addition to a tiltable wing refinement and finally replace the rotor blade grids with an annular grid, in order to use the Actuator Disk (AD) model of the rotor itself. DLR and AHD grids present a slightly less refined surface discretization than ONERA/PoliMI grids.

The dimensions of the grid used are reported in table 2 and the surface grids in AC1 configuration in addition to the Chimera grid system in the CC4 configuration are presented in Figure 4.

All time-accurate calculations have been carried out with a time step corresponding to a 1 degree of rotor revolution, being the rotating speed 2130 rpm for AC1 and 2730 rpm for CC4. They differ by the number of sub-iterations performed in pseudo-time, which have been selected: 20 for ONERA, 50 for PoliMi and 50-100 for DLR, the latter figure referring to the final time period of the computation.

Partner	Turbulence model
ONERA	k-ω Menter with SST correction
DLR	k-ω Wilcox
AHD	k-ω Wilcox and Menter SST
PoliMi	Spalart-Allmaras

Table 1: Employed turbulence models

	ONERA	PoliMi AC1	PoliMi CC4	DLR	AHD
Fuselage and fixed wing	5.8	5.6	5.6	11.7	8.6
Tiltable wing	2	2	2	0.7	0.7
Nacelle	3.8	3.8	5.8	3.6	4.1
Rotor blades *4	4	4	4	2.2	
Actuator disc					0.4
Model support	0.8	0.8	0.8	0.3	1.2
Auxiliary grids			7.5		
Wind tunnel	9.8	9.8	9.8	0.5	2.7
Total	26.2	26	33.5	19	17.7

Table 2: Volume grids dimension, given in number of nodes *10^6

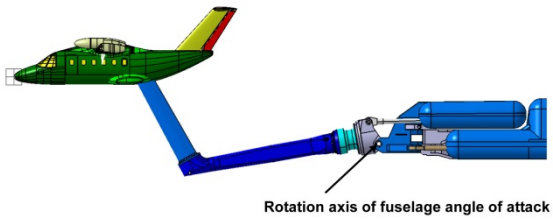

Figure 3: DNW-LLF model support.

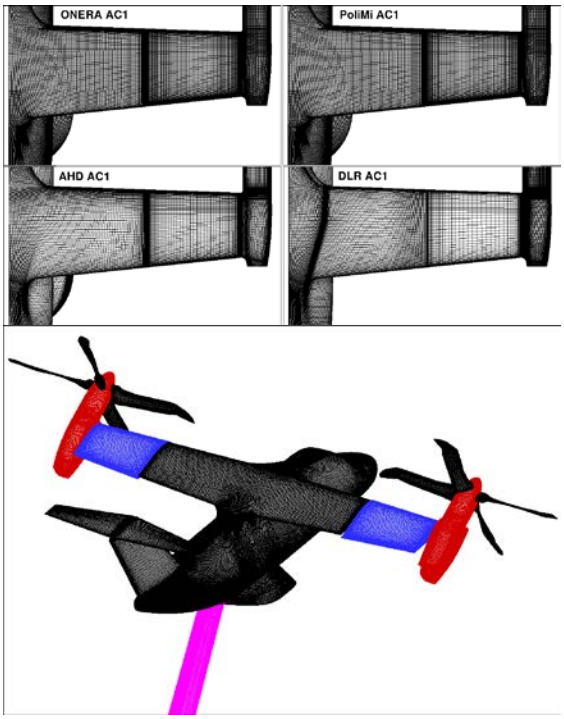

Figure 4: Surface grid on the suction side of the wings and global view of movable parts.

3 Discussion of results

The geometrical and operating conditions for the experimental test cases are shown in Table 3. During the wind tunnel tests, the model was set to the correct configuration (tiltable wing and nacelle angles), then the complete aircraft angle of attack was trimmed to match the target of complete aircraft lift coefficient. In addition, the rotor thrust was trimmed to compensate the complete aircraft drag. Once

the equilibrium is reached, that is to say at the nominal point, all the moveable parts could be moved (nacelle, tiltable wing, elevator, rudder, flaps, flaperons).

The computed results will be analyzed considering the different test cases separately. The cross-sections considered to compare with the measured pressure distributions are described in Figure 5. The upper centreline of the fuselage will be analysed, together with the wing airfoil sections of the inner part of the fixed wing (Y=280mm), the middle of the fixed wing (Y=480mm) and the middle of the tiltable wing (Y=1117mm).

	V(m/s)	Mach	α_0	α_tilt	α_nac	θ_0	θ_1c	θ_1s
AC1	59.1	0.168	9.9	0	0	26	-0.3	1.8
CC4	59.1	0.168	5.3	4	30.1	16.6	0	0

Table 3: Wind tunnel operating condition and model configuration for the selected cases.

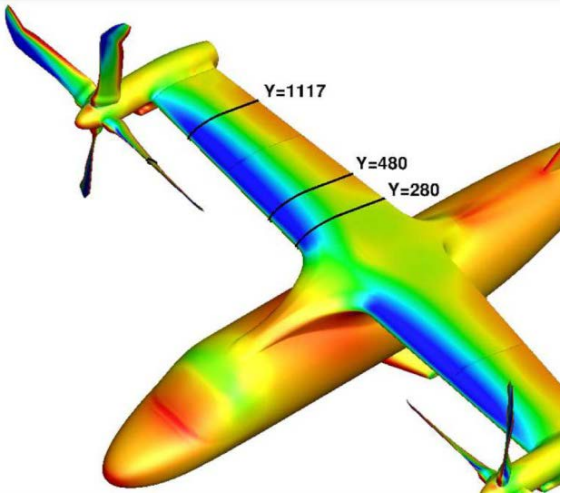

Figure 5: Wing spanwise section for pressure distribution comparison.

3.1 AC1 case

This configuration corresponds to the minimum speed reachable in aircraft-mode. AC1 configuration is characterized by very high incidence and large separation regions on the upper side of the wing, as clearly seen looking at the limiting streamline on the upper surface of the aircraft, Figure 6. ONERA and AHD show a large flow separation on the center of the wing (left part of the wing in Figure 6) and smaller separations on the external part of the wing. We have to notice that only half aircraft is simulated and the symmetrical boundary condition could have an impact on such a flow separation. PoliMi has a small separation in the middle of the wing and DLR has no separation at all, but both have a huge wings gap separation. PoliMi and ONERA have the same 2mm gap and the same grids, so the gap separation predicted by PoliMi could be attributed to the Spalart Allmaras turbulence model. AHD and DLR have the same 1mm wings gap in addition to the k-ω Wilcox turbulence model. The DLR tiltable wing coarse grid could be responsible for this gap separation.

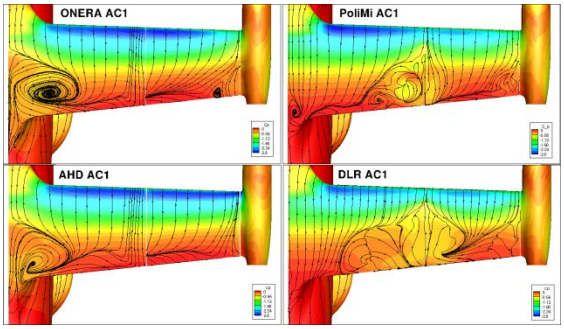

Figure 6: Skin pressure distribution and skin friction lines on the suction side of the wings.

A quantitative assessment can be done considering the upper fuselage centerline pressure distribution (Figure 7). The measured pressures present a plateau that breaks the recompression which occurs after the wing leading edge suction peak. This plateau is very well reproduced in both DNW-LLF and ONERA S1MA measurements and indicates the presence of a recirculation region. The calculations carried out by AHD and ONERA successfully reproduce the presence of the plateau in addition to the suction peak level. PoliMi and DLR predictions, carried out with the Spalart-Allmaras model and the Wilcox two equations model fail in representing the separation and therefore overestimate the suction peak.

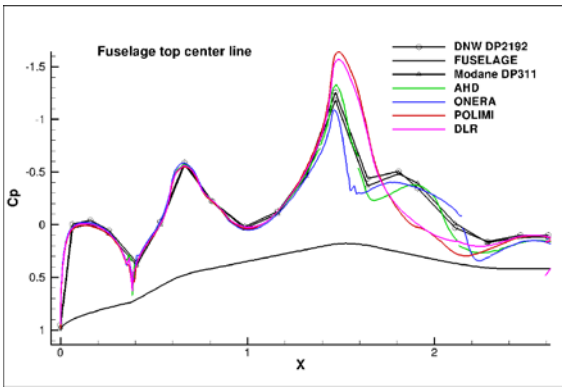

Figure 7: Fuselage top center line pressure coefficient distribution.

Considering the inner part of the fixed wing pressure coefficient distribution presented in Figure 8, a good agreement can be seen between the two wind tunnel measurements. The suction peak is slightly over-valued in DNW but the pressure plateau is clearly visible on the second half part of the wing suction side. From a numerical point of view, the suction peak is very well predicted by the Partners in agreement with Modane measurements, excepted the PoliMi's peak which is slightly over-estimated. The pressure plateau is very well predicted by ONERA, then AHD, and finally DLR and PoliMi have no pressure plateau which is expected and consistent with the flow pattern presented in Figure 6.

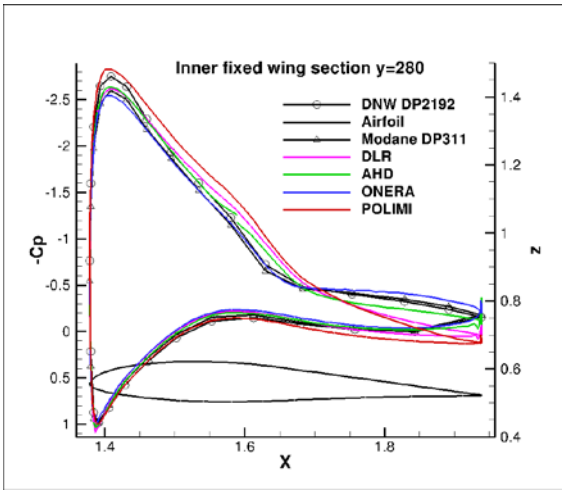

Figure 8: Inner fixed wing pressure coefficient distribution.

In the middle of the fixed wing, Partners have a very good agreement with the pressure coefficient measured in Modane (Figure 9). The DNW suction peak is somewhat over-valued. DLR under-estimates the suction peak but also over-estimates the pressure plateau, in agreement with the gap flow separation visible in Figure 6.

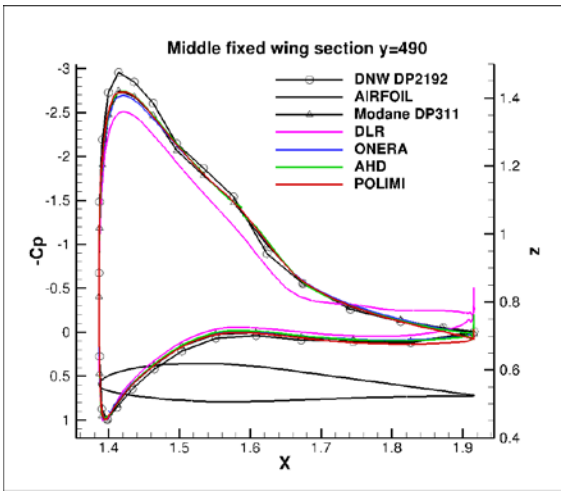

Figure 9: Middle fixed wing pressure coefficient distribution.

Finally, in the middle of the tiltable wing, a good agreement is shown between both wind tunnel measurements, with a DNW suction peak still over-valued, and AHD and ONERA simulations (Figure 10). PoliMi and DLR under-estimate the suction peak, but the trailing edge pressure plateau is well predicted by all the Partners.

As a conclusion on pressure measurements, it can be highlighted that the wing is over-loaded for this very low speed flight configuration. The flow stream on the model is certainly very comparable to ONERA and AHD predictions (Figure 6), that is to say with a large flow separation in the middle of the wings and a trailing edge separation all along the wingspan. Therefore, the flight speed should be increased to avoid that kind of separation in AC1 configuration or the fixed wing flaps should be used to increase the lift.

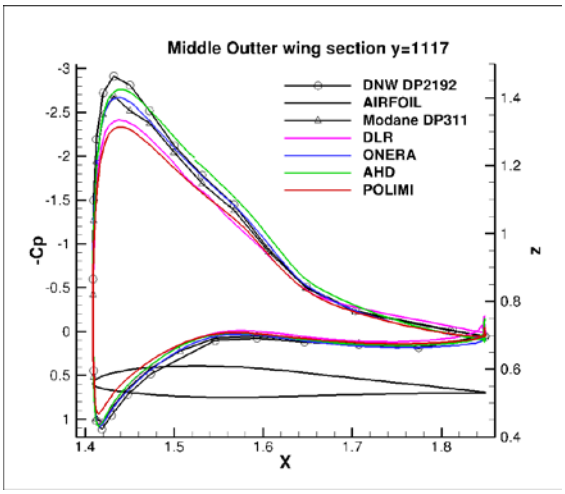

Figure 10: Middle outer wing pressure coefficient distribution.

Loads on the model are more difficult to compare to experiment because of the trimming procedure, but the numerical simulations done by the Partners give us access to more detailed loads. Therefore, we will consider loads on the tiltable wing, the nacelle and the rest of the fuselage with the fixed wing and the empennage.

The tiltable wing lift and drag coefficients clearly show the 4/rev. blade passage effect (Figure 11). DLR and PoliMi have a very similar lift coefficient reinforcing the previous analysis of the similar tiltable wing flow separation (Figure 6 and 10). ONERA also presents a 4/rev. curve but the mean value is slightly higher than DLR and PoliMi, which corroborates the ONERA agreement with experiment on the tiltable wing middle-span pressure coefficient (Figure 10). AHD curve has no 4/rev. shape since the simulation has been done with an actuator disk. The AHD tiltable wing lift coefficient mean value is also in good agreement with the previous pressure coefficient distribution analysis (Figure 10). Finally, the discrepancy between the Partners tiltable wing lift coefficient is 20% of the mean value, which is pretty good considering the large separation on the tiltable wing. The lift fluctuation is between 5% and 7%, depending on the Partner. AC1 tiltable wing is highly loaded because of the 9.9 degrees of incidence, but the blade passage add this 4/rev. load fluctuation leading to wing vibrations.

The drag coefficient also presents the same 4/rev oscillations for Partners simulating the blade passage. The discrepancy between the Partners tiltable wing drag coefficient is about 75% of the mean value which is quite large scatter. Note that the drag average value is small compared to the variance of flow field due to separation around the tiltable wing. The drag fluctuation is between 20% and 30%, depending on the Partner. Finally, wing vibrations are due to a combination of lift and drag fluctuations.

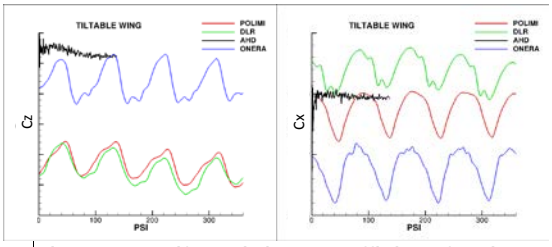

Figure 11: Lift and drag coefficient for the tiltable wing.

The analysis of the nacelle lift and drag coefficients over one rotor revolution (Figure 12) shows that the flow in the nacelle area is very unsteady. The 4/rev. behavior due to the blade passage is clearly visible on PoliMi and DLR plots. ONERA presents a less steady behavior maybe due to the blade root interaction with the nacelle. The discrepancy between the Partners nacelle lift coefficient is only 10% of the mean value and 20% for the drag. The lift fluctuation is 5% and the drag 10%, depending on the Partner. Those values are closer than the tiltrable wing ones since the nacelle is not a lifting surface with flow separations, it is only influenced by the blade passage.

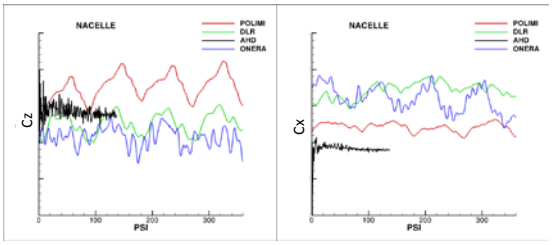

Figure 12: Lift and drag coefficient for the nacelle.

The fuselage and fixed wing lift and drag coefficients plots (Figure 13) also show a 4/rev. behavior due to the blade passage near the fixed wing. ONERA, PoliMi and DLR present

only 5% discrepancy on the fuselage lift whereas AHD lift coefficient is 10% smaller. The fuselage drag coefficients looks even closer although the drag value is very small. The 5% lift fluctuation should correspond to the fixed wing flow separation in the middle of the wing for ONERA and AHD, and near the wing gap for PoliMi and DLR.

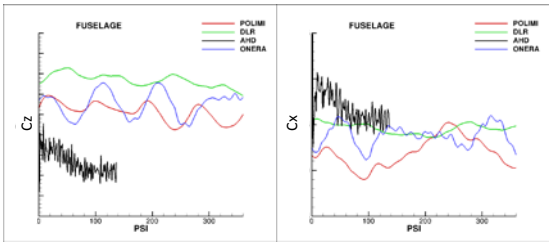

Figure 13: Lift and drag coefficient for the fuselage.

Finally, we plot the complete aircraft lift coefficient taking into account the rotor thrust. This allows us comparing global values between partners to the global balance measurements done in the wind tunnels. There are only 6% discrepancies between the Partners, and the 4/rev. behavior is still present. Partners values are about 15% smaller than the wind tunnel measurements.

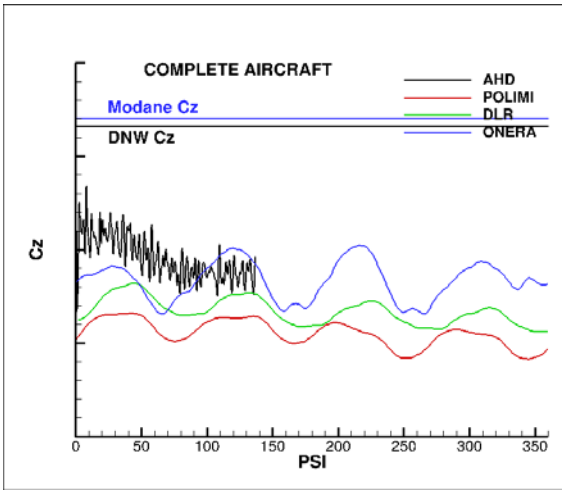

Figure 14: Lift coefficient for the complete aircraft without rotor.

For Partners simulating the rotating blades, we plot the single blade thrust over one rotor revolution (Figure 15). We first remark the very large blade thrust oscillation. This thrust oscillation represents 600% of the mean thrust for PoliMi, 250% for ONERA and 160% for DLR. They are two reasons for this very large thrust oscillations, the first one is the perturbation generated by the highly loaded wing. The flow is going from the wing pressure side to the wing suction side around the nacelle, generating large azimuthal velocity perturbations and therefore angle of attack variations for each blade. The second reason is that the rotor is set at 9.9 degrees of incidence. This also produces angle of attack variations for each blade. These two reasons lead to the large blade thrust oscillation over one rotor revolution. Despite the cyclic law applied during the tests, single blade thrust can be negative. Since the model was neither equipped with lead-lag nor flap hinge, these thrust oscillations lead to large blade root structural constraints.

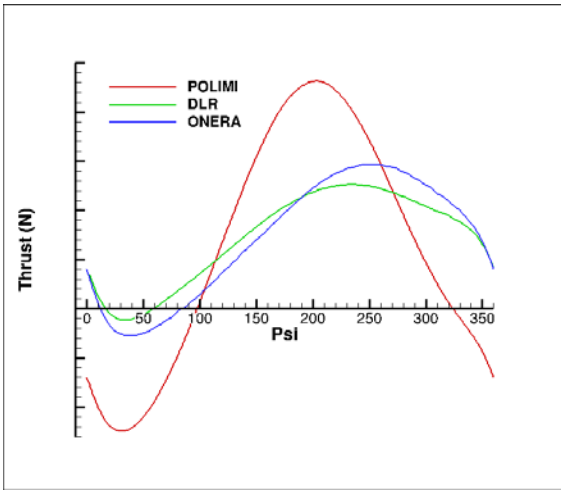

Figure 15: Single blade thrust over one revolution.

Figure 16 presents the total rotor thrust, the sum of the 4 blades thrust over one revolution. ONERA and DLR have trimmed his blade pitch to fit the experimental thrust. PoliMi didn't trimmed the blade pitch and has about 17% less thrust than the other two Partners. The total rotor thrust oscillation is about 15% of the mean value. This rotor thrust fluctuation will lead to nacelle vibrations. The DNW mean thrust value is also indicated.

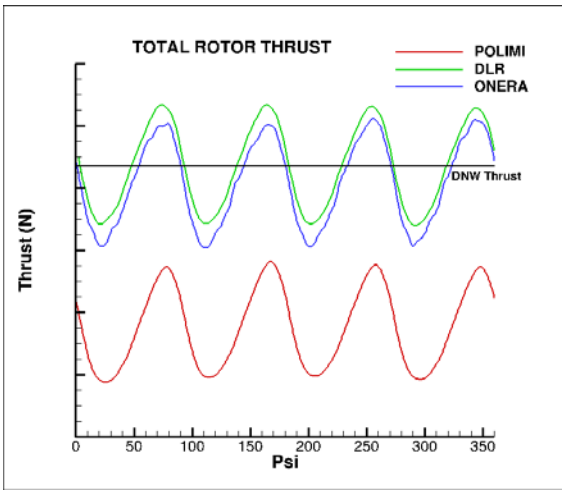

Figure 16: Total rotor thrust over one revolution.

The very low speed aircraft configuration AC1 has shown a good comparison between both DNW-LLF and ONERA S1MA wind tunnels, in addition to Partners simulations in terms of pressure coefficient distributions, despite the large flow separation on the wings. Moreover, the important interaction between the rotor and the wings with its impact on loads fluctuations has been discussed. In order to avoid any flow separation, loads instabilities and aircraft vibrations, we strongly recommend to reduce the aircraft angle of attack and increase the flight speed of the aircraft in this configuration.

3.2 CC4 case

The CC4 conversion configuration differs from the AC1 by the fuselage angle of attack set at 5.3 degrees instead of 9.9 degrees, the tiltable wing angle of 4 degrees compared to the fixed wing, the nacelle angle of 30 degrees with regard to the fixed wing and the rotor thrust value.

Figure 17 presents the skin pressure distribution and skin friction lines on the suction side of the wings. There is no more flow separation in the middle of the wing for ONERA and AHD, thanks to the angle of attack reduction. On the other side, it is surprising that PoliMi predicts a middle wing flow separation as the fuselage and fixed wing angle of attack has been decreased compared to AC1. PoliMi and DLR still have a large wings gap flow separations, in addition to an important interaction with the nacelle, tilted by 26 degrees compared to the tiltable wing. ONERA also has limited interaction with the nacelle and and AHD predicts a flow separation on the full tiltable wing span.

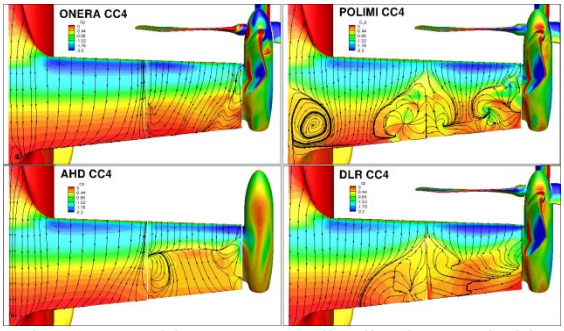

Figure 17: Skin pressure distribution and skin friction lines on the suction side of the wings.

The pressure coefficient on the fuselage center line, plotted in Figure 18, gives a quantitative comparison. There is a good agreement between both wind tunnel measurement in addition to ONERA, DLR and AHD. PoliMi is the only Partner presenting a pressure plateau coming from the middle wing flow separation.

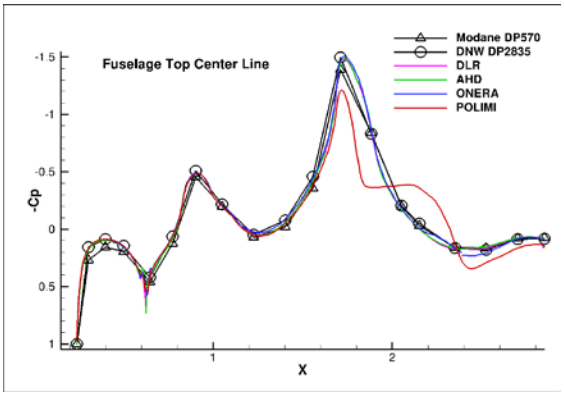

Figure 18: Fuselage top center line pressure coefficient distribution.

Concerning the inner fixed wing pressure coefficient distribution (Figure 19), we remark that the pressure peak measured in DNW is higher than the one measured in Modane. In DNW the CC4 configuration, corresponding to data point 2835 has been trim to a lift 25% higher than the Modane lift. Despite this point, there is a good agreement between Partners simulations and all Partners pressure distributions are in between Modane and DNW ones. In addition, no pressure plateau can be seen neither in experimental values nor in numerical ones, confirming the absence of flow separation in this part of the wings. The same

analysis can be done for the middle of the inner wing section (Figure 20).

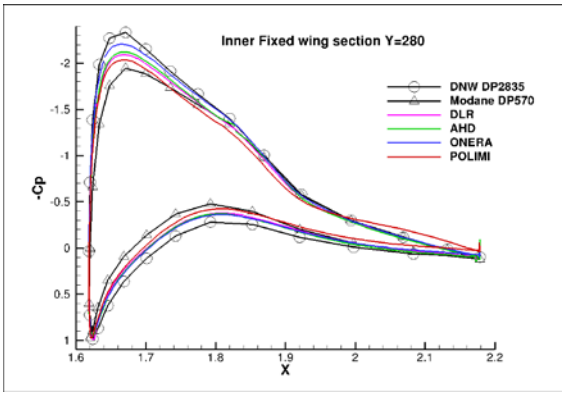

Figure 19: Inner fixed wing pressure coefficient distribution.

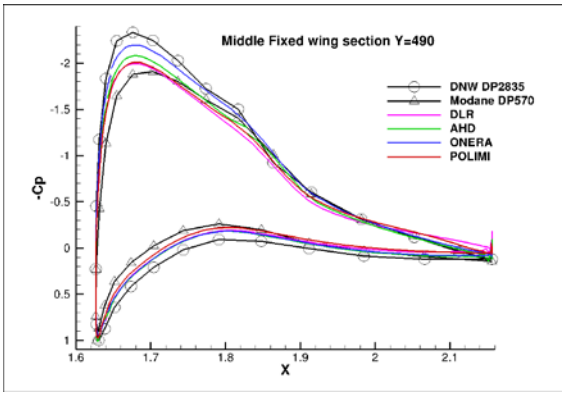

Figure 20: Middle fixed wing pressure coefficient distribution.

In the middle of the tiltable wing (Figure 21) measurements are not so clear concerning the pressure plateau. It seems that the flow is not as well attached as it is on the fixed wing. AHD presents a very large pressure plateau corresponding to the tiltable wing flow separation seen in Figure 16. PoliMi and DLR also predict a pressure plateau but smaller than AHD. ONERA is in good agreement with pressure measurements. This last point indicates that there is no recirculation but a strong influence of the nacelle tilted by 26 degrees compared to the tiltable wing.

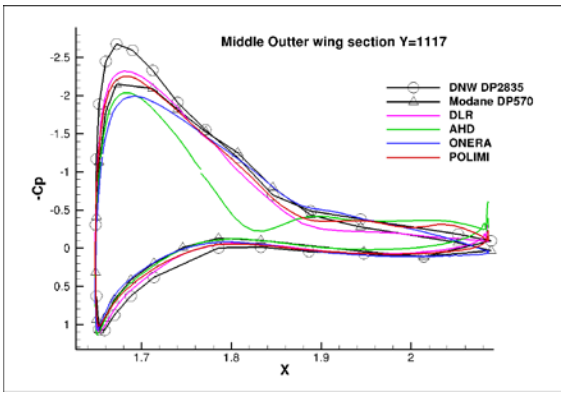

Figure 21: Middle outer wing pressure coefficient distribution.

The global loads on the tiltable wing over one revolution plotted in Figure 22 shows a 4/rev. behavior, even if the influence of the blades passage is not as clear as for AC1 and is disturbed by the vicinity of the nacelle. AHD simulation with actuator disk also presents strong oscillations that can be attributed to the wing-nacelle interaction. The discrepancy between the Partners tiltable wing lift coefficient is 20% of the mean value, which is not so bad considering the wing-nacelle interaction. The lift fluctuation is between 12% and 16%, depending on the Partner.

The drag coefficient does not present clear 4/rev. oscillations for Partners simulating the blade passage and AHD simulation also presents unsteadyness. The discrepancy between the Partners tiltable wing drag coefficient is important since ONERA and DLR predict a very small drag whereas AHD drag is twice larger.

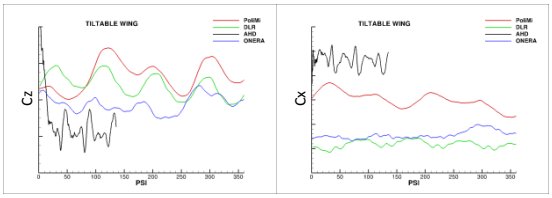

Figure 22: Lift and drag coefficients for the tiltable wing.

Concerning the nacelle (Figure 23), the 4/rev. lift coefficient oscillation due to the blade passage is clear. AHD does not have 4/rev. oscillation because of the actuator disk modelisation of the rotor. Moreover, the AHD nacelle lift coefficient is 30% smaller than the Partners simulating the blade passage, who only have 15% discrepancy on the nacelle lift

coefficient. This point underlines the strong influence of the blade on the nacelle loads.

PoliMi, AHD and DLR have a pretty good agreement on the nacelle drag coefficient with only 25% of discrepancy, whereas ONERA predict a nacelle drag 80% higher than the other Partners.

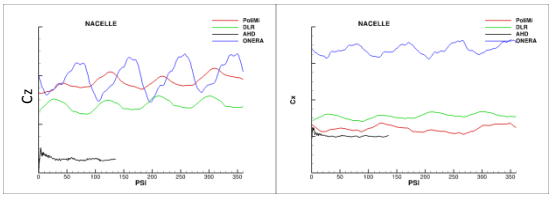

Figure 23: Lift and drag coefficient for the nacelle.

The 4/rev. blade passage influence on the fuselage and fixed wing is clearly visible for PoliMi prediction (Figure 24). This is certainly due to the large flow separation on the center of the wing in addition to the wings gap separation that make the fixed wing more sensitive to the blade passage. DLR also presents a 4/rev. behavior whereas ONERA simulation seems less fluctuating despite the lack of fixed wing separation. The same analysis can be done for AHD lift coefficient which seems very unsteady despite the lack of fixed wing flow separation. There is about 30% discrepancy on the fuselage lift coefficient among the Partners. On the drag coefficient the discrepancy is higher because ONERA and DLR predict small values, PoliMi intermediate ones, and AHD very high drag.

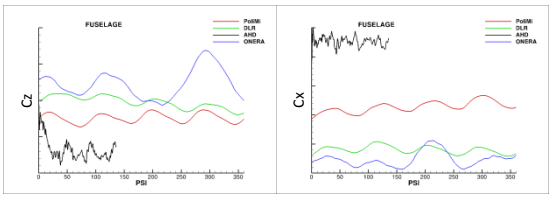

Figure 24: Lift and drag coefficient for the fuselage.

For Partners simulating the blades rotation, we plot the single blade thrust over one rotor revolution (Figure 25). We remark again the very large blade thrust oscillation. This thrust oscillation represents 790% of the mean thrust for PoliMi, 600% for ONERA and 420% for DLR. In this conversion case, the main reason for these huge thrust oscillations is the 30 degrees of nacelle angle in addition to the 5.3 degrees of fuselage angle of attack. This produces large angle of attack variations for each blade. In addition, the CC4 test point has been done without cyclic pitch angles. Since the model was neither equipped with lead-lag nor flap hinge, these thrust oscillations lead to large blade root structural constraints. An adapted cyclic law could reduce the single blade thrust variation and thus help reducing the blade root structural constraints.

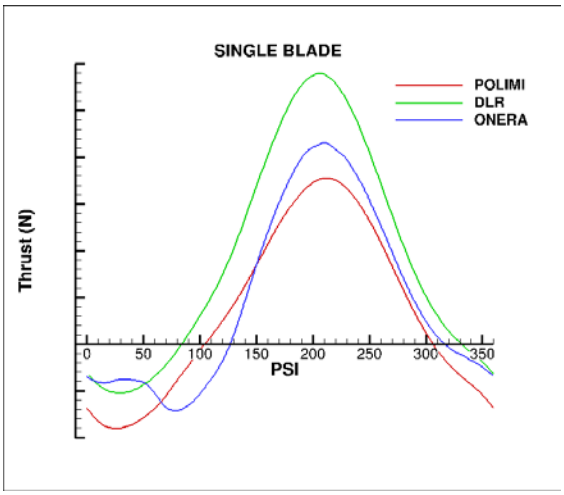

Figure 25: Single blade thrust over one revolution.

Figure 26 presents the total rotor thrust, ONERA has trimmed his blade pitch to obtain acceptable thrust. PoliMi has about 27% less thrust than ONERA and DLR has about 100% more thrust than ONERA. The total rotor thrust oscillation is about 15% of the mean value for ONERA and PoliMi, whereas it is only 5% for DLR. This rotor thrust fluctuation will lead to nacelle vibrations. The DNW mean thrust value is also indicated.

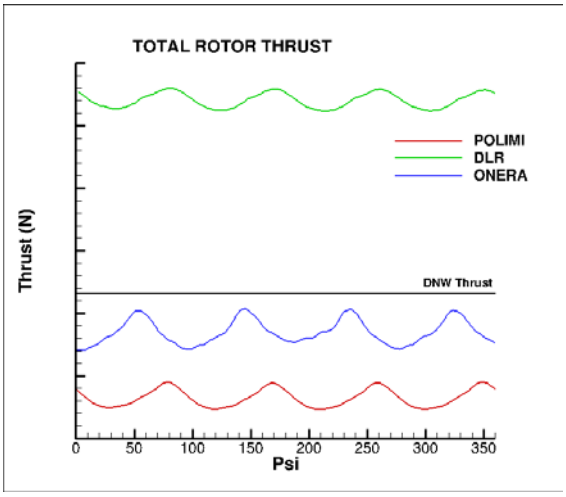

Figure 26: Rotor thrust over one revolution.

Finally, we present in Figure 27 the Q-criterion iso-surface for the CC4 configuration. This figure illustrates the important aerodynamic interactions existing between each blade passage in front of the nacelle, the tiltable wing, but also with the fixed wing.

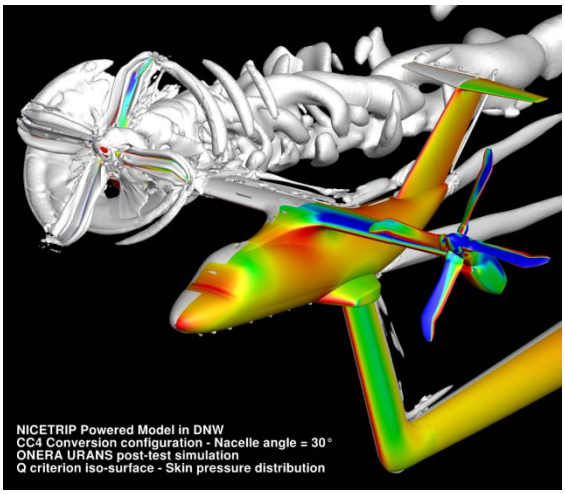

Figure 27: Q criterion iso-surface for the CC4 conversion case.

4 Conclusions

A huge data base is now available thanks to the wind tunnel test done in the DNW-LLF and ONERA S1MA wind tunnels. The wind tunnel tests cover the full aircraft flight domain, with the conversion corridor from helicopter mode to very low speed aircraft mode in addition to speed increase until the maximum flight speed at Mach=0.55. Two configurations only have been simulated by the mean of CFD with different codes, turbulence models and grids: the very low speed aircraft configuration AC1 and the conversion configuration CC4. In both test cases, a good agreement with experimental measurement is obtained, especially for pressure coefficient distributions.

It has been shown that the AC1 test case presents a large flow separation on the wing because of too low speed flight for high angle of attack. Both test cases had shown very important interactions between the blade passage in the region of the nacelle, the tiltable wing and the fixed wing. These important interactions lead to 4/rev. fluctuating loads and then aircraft vibrations. Finally, the CFD is the unique method able to capture all the aerodynamic interactions generated by the tiltrotor flight. Therefore, additional test cases should be computed and compared to the experimental data base available in order to give a better understanding of the tiltrotor aerodynamic behavior.

Aknowledgements:

This work has been partially funded under the EC supported FP6/Aeronautics Project AIP5-CT-2006-03-944 NICETRIP.

References

[1] L. Vigevano, M. Biava, P. Beaumier, J. Decours, W. Khier, and T. Kneisch. Code to code comparison of aircraft-mode tilt-rotor aerodynamics. In 38th European Rotorcraft Forum, Amsterdam, the Netherlands, 2012.

[2] L. Cambier, S. Heib, S. Plot. The Onera elsA CFD software: input from research and feedback from industry" Mechanics and Industry TP 2013-437.

[3] N. Kroll, B. Eisfeld, and H.M. Bleecke. The Navier-Stokes Code FLOWer. In Notes on Numerical Fluid Mechanics, Vieweg, Braunschweig, volume 71, pages 58–71, 1999.

[4] M. Biava. RANS computations of rotor/fuselage unsteady interactional aerodynamics. PhD thesis, Dipartimento di Ingegneria Aerospaziale, Politecnico di Milano, 2007.

[5] J.C. Kok. Resolving the dependence on freestream values for the k-ω turbulence model. AIAA J., 38:1292–1295, 2000.

[6] D.C. Wilcox. Reassessment of the scaledetermining equation for advanced turbulence models. AIAA J., 26:1299–1310, 1988.

[7] F. R. Menter. Zonal two equation k-ω turbulence models for aerodynamic flows. AIAA Paper, (93-2906), 1993.

[8] P.R. Spalart and S.R. Allmaras. One equation model for aerodynamic flows. In 30th AIAA Aerospace Science Meeting & Exhibit, Reno, NV.AIAA 92-0439, 1992.